

## Chapter 2

# Experimental Methods

### 2.1 Bulk Crystal Growth

#### 2.1.1 Polycrystal Samples

Polycrystalline samples of B20-type germanides were synthesized with a cubic-anvil-type high-pressure apparatus (see also Ref. [1]). A mixture of elemental materials with an atomic ratio of  $T : \text{Ge} = 1 : 1$  was at first arc-melted in an argon atmosphere. (Here,  $T$  represents transition-metal element.) The alloy was placed in a cylindrical BN capsule (Fig. 2.1) and was heat-treated for 1 hour at 1073 K under a high pressure of 4.0 GPa. Some samples include a trace of impurity less than 4 % in volume fraction.

Figure 2.2 shows some powder X-ray diffraction (XRD) patterns and composition dependence of lattice constant of synthesized B20-type germanides. Monotonous change in the lattice constant indicates good solubility of the transition-metal elements.

#### 2.1.2 FeGe Single Crystal

A single crystal of FeGe was grown by chemical vapor transport (CVT) method. A mixture of Fe and Ge powders with an atomic ratio of 1 : 1 was put into a cylindrical quartz tube, which was evacuated below  $1 \times 10^{-4}$  Torr. The evacuated tube was heated at 700 °C for 1 day. The obtained powder mainly consists of FeGe with B35 crystal structure. The powder of B35-type FeGe was placed with  $\text{I}_2$  (20 mg) in an evacuated cylindrical quartz tube whose volume is  $\pi 10^2 \times 120 \text{ mm}^3$ . The sample was placed in a three-zone furnace and heated for 1 month with a thermal gradient: 560 °C at an end of cylinder where powder sample was placed and 500 °C at the other end of the cylinder. Many pieces of B20-type FeGe single crystals were grown

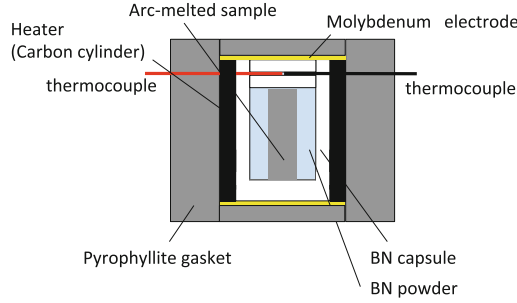


**Fig. 2.1** Cross-section drawing of assembly for high-pressure synthesis. A high pressure is applied in six directions of the cubic gasket surface

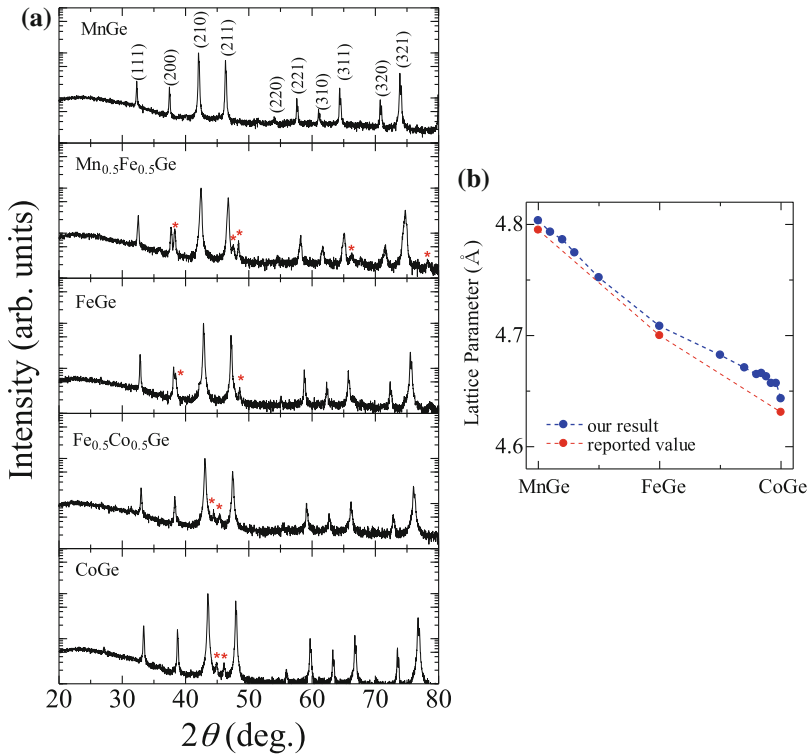


**Fig. 2.2** **a** Several X-ray diffraction patterns of the synthesized B20-type germanides. *Red* asterisks indicate intensities from impurity. **b** Calculated lattice constants from the XRD patterns in comparison with previous reports [1]. A linear relation between the composition ratio and the lattice constant verifies good solubility of Mn, Fe, and Co

at the lower temperature side of the cylinder. Typical size of the crystals is 0.7 mm. The crystals have cleavage planes. Figure 2.3 shows the single crystal with (111) cleavage plane, which was used for measurements.

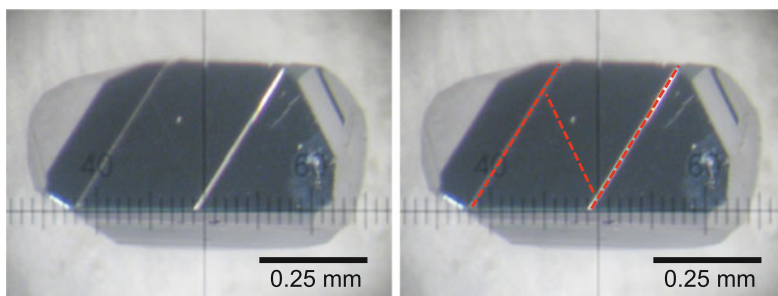


**Fig. 2.3** B20-type FeGe single crystal grown by CVT method. The wide surface is a cleavage plane of (111) surface with small steps (red dashed lines) forming regular triangles

## 2.2 Thin-Film Growth

FeGe epitaxial films with 40-nm thickness were grown on highly-resistive Si(111) substrates ( $\rho > 1000 \, \Omega \, \text{cm}$ ) by molecular beam epitaxy. Figure 2.4 shows lattice matching between FeGe(111) surface and Si(111) surface. Fe(Ge) atoms on the green and purple triangles indicated in Fig. 2.4b, d are stacked on corresponding Si atoms indicated in Fig. 2.4c. The lattice mismatch is  $-0.05 \, \%$ .

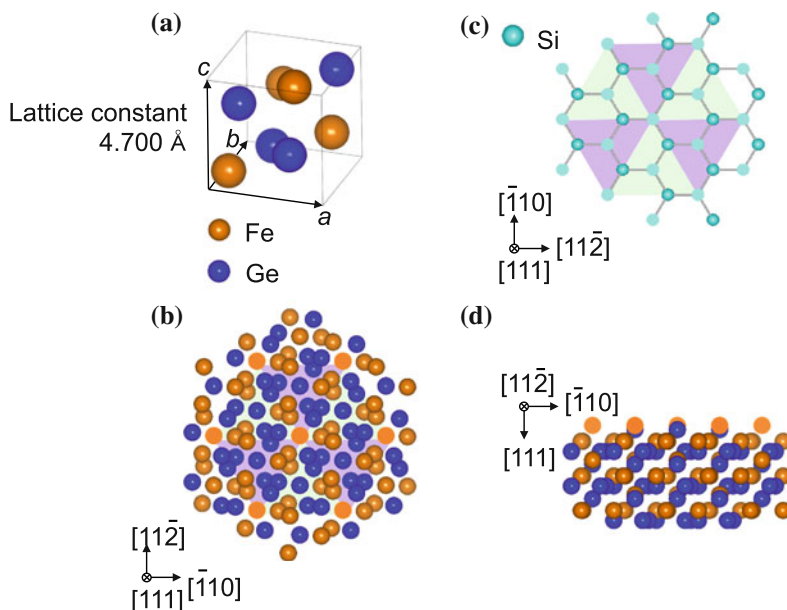


**Fig. 2.4** Schematics of atomic arrangements of **a** a unit cell of FeGe, **b** FeGe viewed from  $[111]$  crystal axis, **c** Si viewed from  $[111]$  crystal axis, and **d** FeGe viewed from  $[112]$  crystal axis

Fe and Ge were deposited on the wafer using Knudsen cells. We deposited Fe and Ge onto a Si(111)- $7 \times 7$  surface heated at 325 °C by using Knudsen cells until a prescribed thickness was reached. The characteristic  $\sqrt{3} \times \sqrt{3}$  reflection high-energy electron diffraction (RHEED) pattern on the B20-compound (111) surface appeared during the deposition. The single phase nature was confirmed by  $2\theta$ - $\theta$  XRD.

## 2.3 Magnetization and Electrical Transport Measurement

Samples for magnetization and electrical transport measurements were cut into rectangular shape with a typical size of  $4 \times 1.5 \times 0.2 \text{ mm}^3$ . Magnetization and electrical transport measurements were performed using Quantum Design Physical Property Measurement System (PPMS) and Magnetic Property Measurement System (MPMS). Resistivity was measured with a four-probe method. Measurements of magnetoresistance and Hall resistivity were performed with the current parallel to the longest side ( $x$  axis) and the magnetic field to the shortest one ( $z$  axis). Electrical contacts were made with indium. Magnetization ( $M$ ) was measured with the same magnetic field direction as the transport measurements.

## 2.4 Neutron Scattering

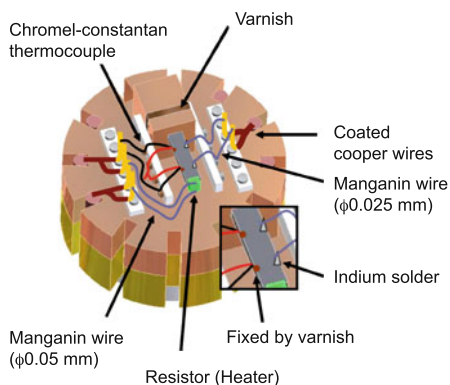
High-angle powder neutron diffraction experiments on MnGe were performed using HERMES and TAS-2 installed at the JRR-3 reactor of Japan Atomic Energy Agency (JAEA). Wavelengths of used neutron beams at HERMES and TAS-2 are 1.8449(1) Å and 2.359 Å, respectively. The powder sample includes a trace of impurity less than 4 % in volume fraction.

Small-angle neutron scattering experiments on MnGe were carried out using SANS-I instrument at the Paul Scherrer Institut using neutrons with wavelength 4.7 Å. The same powder sample was packed in a single-crystalline silicon container with a height of 9.5 mm and a diameter of 18 mm, and installed in a cryomagnet. The magnetic field was applied perpendicular to the incident neutron beam collimated over 4.5 m. The diffracted neutrons were collected by a two-dimensional multidetector placed 2 m behind the sample.

## 2.5 Thermal Transport Measurement

Seebeck coefficients and thermal conductivities were measured in a setup placed in a vacuum ( $< 1 \times 10^{-4}$  Torr) (Fig. 2.5). One end of the sample was fixed to a copper block as the heat bath by silver epoxy, and the other to an 10 kΩ resistor through which electric current was passed to generate heat current. Chromel–constantan

**Fig. 2.5** Setup for thermal transport measurement



thermocouples were attached to a sample by varnish. The thermal electromotive force was measured using manganin wires, whose Seebeck coefficient is negligible small (less than  $1 \mu\text{V/K}$  below 300 K) [2].

## References

1. H. Takizawa, T. Sato, T. Endo, M. Shimada, J. Solid State Chem. **73**, 40 (1988)
2. K.D.D. Rathnayaka, J. Phys. E: Sci. Instrum. **18**, 380 (1985)

Charge and Heat Transport Phenomena in Electronic  
and Spin Structures in B20-type Compounds

Kanazawa, N.

2015, XII, 89 p. 60 illus., 52 illus. in color., Hardcover

ISBN: 978-4-431-55659-6